

NJC

Accepted Manuscript



This is an *Accepted Manuscript*, which has been through the Royal Society of Chemistry peer review process and has been accepted for publication.

Accepted Manuscripts are published online shortly after acceptance, before technical editing, formatting and proof reading. Using this free service, authors can make their results available to the community, in citable form, before we publish the edited article. We will replace this *Accepted Manuscript* with the edited and formatted *Advance Article* as soon as it is available.

You can find more information about *Accepted Manuscripts* in the [Information for Authors](#).

Please note that technical editing may introduce minor changes to the text and/or graphics, which may alter content. The journal's standard [Terms & Conditions](#) and the [Ethical guidelines](#) still apply. In no event shall the Royal Society of Chemistry be held responsible for any errors or omissions in this *Accepted Manuscript* or any consequences arising from the use of any information it contains.

New Insight into High-Temperature Driven Morphology Reliant CoMoO₄ Flexible Supercapacitor

**John Candler^a, Tyler Elmore^a, Bipin Kumar Gupta^b, Lifeng Dong^c, Soubantika
Palchoudhury^d, Ram K. Gupta^{a*}**

^aDepartment of Chemistry, Pittsburg State University
1701 S. Broadway, Pittsburg, KS 66762, USA

^bNational Physical Laboratory (CSIR), Dr K.S. Krishnan Road, New Delhi 110012, India

^cPhysics, Astronomy, and Materials Science, Missouri State University
901 S. National Avenue, Springfield, MO 65897

^dCenter for Materials for Information Technology, The University of Alabama, Tuscaloosa, AL-
35487

* Corresponding author. Tel.: +1 620 2354763; fax: +1 620 2354003
E-mail address: ramguptamsu@gmail.com(R.K. Gupta).

New Insight into High-Temperature Driven Morphology Reliant CoMoO₄ Flexible Supercapacitor

Abstract:

A facile hydrothermal method has been successfully developed for the synthesis of cobalt molybdate (CoMoO₄). The morphology of the CoMoO₄ was tailored by varying growth conditions and as a result different morphologies have been achieved such as cauliflower, brick and nano-sphere structures. The proposed potential use of the CoMoO₄ as an electrode material for flexible supercapacitor applications was examined by cyclic voltammetry (CV) and galvanostatic charge-discharge measurements. It was observed that the specific capacitance of the CoMoO₄ depends on its morphologies. The specific capacitance of 169 F/g in 3M KOH at the current of 1 mA was observed for the nano-sphered CoMoO₄. The effect of electrolytes (LiOH, NaOH and KOH) on the electrochemical properties of the CoMoO₄ was also investigated. The specific capacitance depends on the type of electrolytes and showed the highest value of 259 F/g in 3M NaOH electrolyte. Furthermore, these electrodes showed excellent cyclic stability. We have fabricated flexible supercapacitor device by sandwiching two electrodes separated by an ion transporting layer. The device shows no degradation in the capacitive properties on bending and shows improved stability with number of cyclic CV performance. The effect of temperature on the charge storage properties of the device was also investigated for high temperature applications. The specific capacitance of the device significantly increased when the operational temperature of the device was elevated from 10 to 70 °C. Hence, this work provides an ultimate facile method to synthesize morphologies controlled cobalt molybdates for the applications in next generation flexible energy storage devices which could drive more efficiently at higher temperature.

KEYWORDS: CoMoO₄, hydrothermal synthesis, cyclic voltammetry, supercapacitor, cyclic stability

1. Introduction

Supercapacitors are considered the most prominent and efficient energy storage devices, next to lithium ion batteries due to their high power densities, fast charge-discharge capabilities and long cyclability.¹⁻⁶ Supercapacitors possess high power density in compare to batteries and these are able to solve the increasing demand for energy in small consumer products, electrical vehicles and devices where quick power delivery is highly desired.⁷⁻¹⁰ Supercapacitors are classified into two categories based on their charge storage mechanism. The first group capacitors are called as electrical double-layer capacitors (EDLCs), where the charge is stored at the interface. The second group is recognized as redox electrochemical capacitors (pseudocapacitors), where the charge storage arises due to Faradaic reactions at electrode/electrolyte interface.^{1, 11} Although the pseudocapacitors have higher charge storage capacity compare to EDLCs but suffer from high cost and poor cyclic stability. Since, the charge-storage capacity of pseudocapacitors are largely depends on the redox process at the electrode/electrolyte interface and their performance, which could be improved by using nano-structured redox active materials.¹²⁻¹⁴

Several redox active metal oxides and sulfides such as iron oxide, nickel oxide, ruthenium oxide, cobalt oxide, manganese oxide, molybdenum sulfide and cobalt sulfide have been used for supercapacitor applications.¹⁴⁻²⁸ Recently, metal molybdates have attracted considerable research interests for supercapacitor applications due to their excellent electrochemical performance, low cost and environmental friendliness.²⁹ Mai et al³⁰ have synthesized three-dimensional $\text{MnMoO}_4/\text{CoMoO}_4$ hetero-structures. These hetero-structures showed a specific capacitance of 187.1 F/g at a current density of 1 A/g with good reversibility

and cyclic efficiency. The electrochemical properties of nanorods and hierarchical nanospheres of NiMoO₄ were well studied and compared with respect to their morphology.³¹ The nanospheres of NiMoO₄ showed a higher specific capacitance and better cycling stability due to their large surface area and high electrical conductivity.

Xia et al³² have used a facile hydrothermal method to synthesize CoMoO₄/graphene for supercapacitor applications. The CoMoO₄/graphene composite showed a specific capacitance of about 394.5 F/g from the CV curve at 1 mV/s, which was higher than that of pure-CoMoO₄ (72.0 F/g). A facile sonochemical method was also used for the synthesis of CoMoO₄ nanostructures for supercapacitor applications.³³ The CV curves showed the presence of redox pairs, which confirms the pseudocapacitance nature of the CoMoO₄. The galvanostatic charge-discharge studies showed a maximum specific capacitance of 133 F/g at a constant discharge current density of 1 mA/cm². Microwave assisted synthesis of reduced graphene oxide-cobalt molybdate (RGO/CoMoO₄) nano-composites was reported.³⁴ The resulting nanocomposites showed well anchored CoMoO₄ nanoparticles on graphene sheets. The specific capacitance of CoMoO₄ improved from 95.0 F/g to about 322.5 F/g by making nanocomposite with reduced graphene oxide.

Recently, Liu et al³⁵ have studied the effect of calcination temperature on the electrochemical properties of CoMoO₄. It was observed that high crystallinity induced by calcination at high temperature is unfavorable to improve the supercapacitive performance of the CoMoO₄. In present study, we report a detailed investigation on the effect of morphology on the charge storage capacity of CoMoO₄. CoMoO₄ were grown under different conditions to tailor the morphology using a facile hydrothermal method. The results obtained from the electrochemical study suggest that the charge storage capacity largely depends on morphology of the CoMoO₄.

The highest specific capacitance of 259 F/g with excellent cyclic and flexibility stability was observed. The effect of temperature of the capacitive properties of the supercapacitor device was tested from 10-70 °C. It was observed that device works better at higher temperature. The electrochemical results strongly suggest potential application of cobalt molybdate as a flexible electrode material for high performance and stable supercapacitor which is requirement of today's need.

2. Experimental details

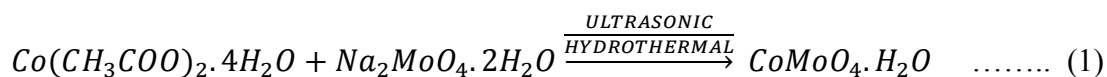
$\text{Na}_2\text{MoO}_4 \cdot 2\text{H}_2\text{O}$ and $\text{Co}(\text{CH}_3\text{COO})_2 \cdot 4\text{H}_2\text{O}$ of analytical grade were used in experiments without further purification. Other chemicals such as ethanol and ethylene glycol were also of analytical grade. In typical synthesis, 1 mmol $\text{Na}_2\text{MoO}_4 \cdot 2\text{H}_2\text{O}$ and 1 mmol $\text{Co}(\text{CH}_3\text{COO})_2 \cdot 4\text{H}_2\text{O}$ were dissolved in 30 ml water (CMO-1), 30 ml (1:1 v/v) ethanol-water mixture (CMO-2) and 30 ml ethylene glycol (CMO-3) using ultrasonication bath. Then, the obtained solution was placed into a 50 mL autoclave with a Teflon liner. The autoclave was maintained at 150 °C for 12 hours. Subsequently, the autoclave was cooled naturally in air. The resulting black precipitates were filtered, washed with distilled water for several times and dried at 500 °C for 4 hours.

The structural characterizations of the cobalt molybdate powder samples were performed using X-ray diffraction (XRD) and scanning electron microscopy (SEM). The XRD patterns were recorded with Shimadzu X-ray diffractometer using the 2θ - θ scan with $\text{CuK}\alpha_1$ ($\lambda=1.5406$ Å) radiation which operated at 40 kV and 30 mA. The particle size and morphology of the cobalt molybdates were studied using a JEOL JSM-840A scanning electron microscope and an FEI Quanta 200 field emission scanning electron microscopy (FESEM) equipped with an Oxford INCA 250 silicon drift X-ray energy dispersive spectrometer (EDS).

The electrochemical measurements were performed using standard three electrode system on a Versastat4-500 electrochemical workstation (Princeton Applied Research, USA). The working electrode was prepared by mixing 80 wt.% of the synthesized cobalt molybdate powder, 10 wt.% of acetylene black and 10 wt.% of polyvinylidene difluoride (PVdF) in the presence of N-methyl pyrrolidinone (NMP). After mixing the components, the slurry was pasted onto nickel foam. The prepared electrode was dried at 60°C under vacuum for 10 h. The loading mass of CMO-1, CMO-2 and CMO-3 was 1.78, 1.22 and 2.28 mg, respectively. The loading mass of cobalt molybdate was accurately measured by weighing the nickel foam before and after electrode preparation using an analytical balance (model MS105DU, Mettler Toledo, max. 120g, 0.01mg of resolution). A platinum wire and a saturated calomel electrode (SCE) was used as a counter electrode and a reference electrode, respectively. 3M KOH, NaOH and LiOH were used as electrolytes. The performance of the supercapacitors was evaluated by cyclic voltammetry (CV) and galvanostatic charge-discharge techniques. The flexible device was assembled using two working electrodes separated by ion transporting layer (Celgard, 25µm thick, 39% porosity) in NaOH electrolyte. Before assembling the device, both working electrodes and ion transporting layer were soaked in the electrolyte for 1 hr.

3. Results and discussion

The morphologies controlled synthesis of cobalt molybdate were performed using ultrasonic assisted hydrothermal method. The chemical reaction for formation of cobalt molybdate is given below:



The synthesized cobalt molybdate and the fabricated electrodes were structurally and electrochemically characterized for their potential applications as a flexible electrode for supercapacitors. In the following sections, we present the details of our observations and discussions.

The crystal structure and phase purity of the cobalt molybdates were studied using XRD measurement. The X-ray diffraction patterns of the synthesized cobalt molybdates are shown in Fig. 1. The diffraction peaks at 13.22, 19.18, 23.34, 25.46, 26.51, 27.26, 28.48, 32.14, 32.87, 33.76, 36.74, 38.78, 40.27, 41.65, 43.75, 45.14, and 47.44 can be assigned to the reflections of the (001), (201), (021), (201), (002), (112), (311), (131), (022), (222), (400), (040), (003), (222), (223), (113), and (421) planes, respectively. The XRD patterns are in good agreement with the standard pattern of CoMoO_4 (JCPDF, card no. 21-0868). The absence of any other impurity peaks except CoMoO_4 peaks suggests that the synthesized materials are phase pure.

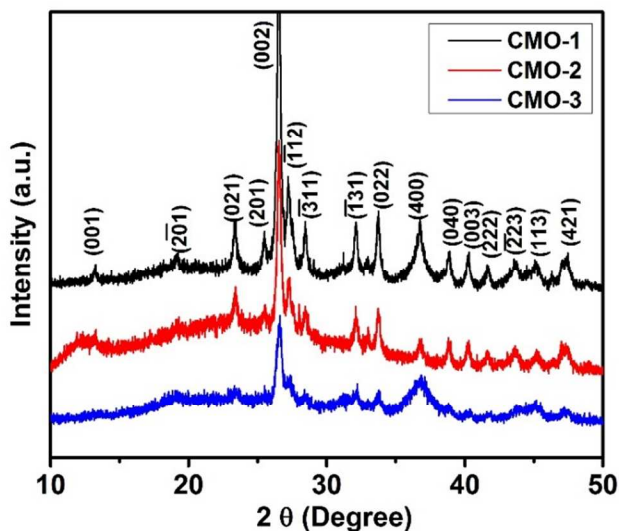


Fig. 1: XRD patterns of synthesized cobalt molybdate of different morphologies.

Furthermore, the effect of growth conditions on the morphology and size of cobalt molybdate were studied in details using scanning electron microscopy. SEM images of the cobalt molybdate grown under different conditions are shown in Fig 2. As seen in the SEM images, the structure and morphology of the CMO largely depend on the growth conditions. The cobalt molybdate synthesized in water shows morphology like cauliflower (CMO-1) whereas just by changing the water to ethanol-water (1:1 v/v) mixture the morphology looks like solid bricks (CMO-2). Interestingly, using ethylene glycol as solvent, the morphology of cobalt molybdate changes to nanostructure (CMO-3) with high porosity. The nanostructure of the synthesized cobalt molybdate in ethylene glycol is also revealed in XRD analysis. The broad peaks observed in the XRD patterns of the CMO-3 suggest its nano structure. The nanostructured materials show higher full width half maximum in the XRD patterns compared to the microstructured materials. TEM measurements were conducted to further investigate the microstructural properties of the cobalt molybdates. Fig. 3 shows the TEM images of CMO-1, CMO-2 and CMO-3 respectively. The TEM results reveal that the cobalt molybdates are associated with porous morphology. Energy dispersive X-ray spectroscopy (EDS) of the CMO-3 shows the presence of Co, Mo, O, C, and Cu (Fig. 1S). The presence of Cu is due to the conductive copper tape used in EDS measurement. The relative concentration ratio of Co, Mo and O was observed to be about 1:1:4, which further confirms the CoMoO_4 phase.

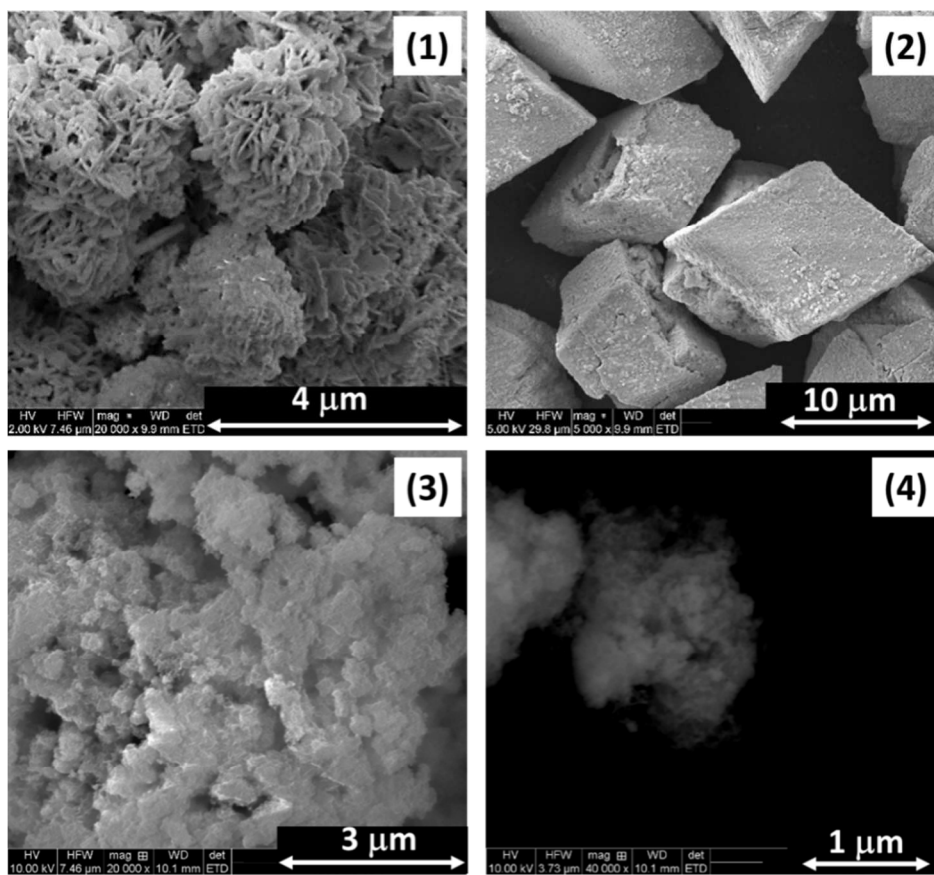


Fig. 2: SEM images of (1) CMO-1, (2) CMO-2, (3) CMO-3 and (4) magnified view of CMO-3.

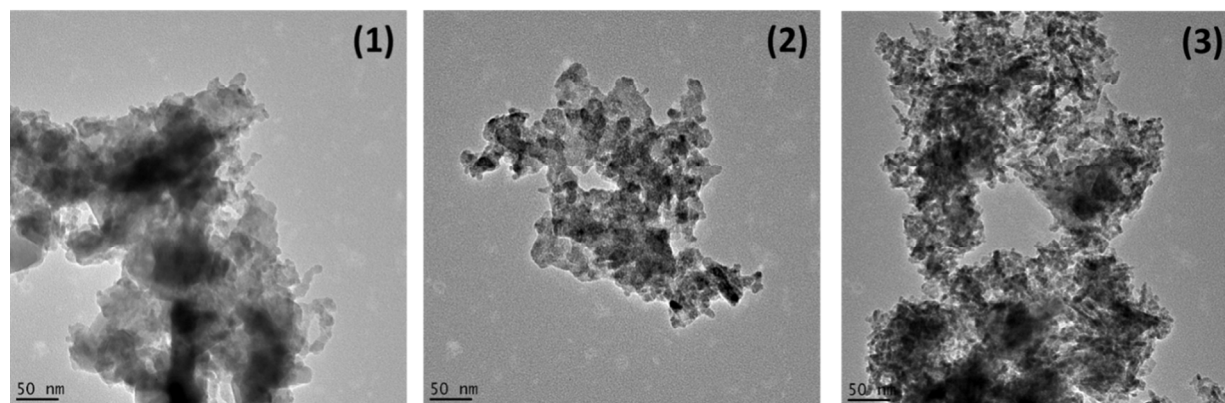


Fig. 3: TEM images of (1) CMO-1, (2) CMO-2 and (3) CMO-3.

Further, the effect of morphology on the charge storage capacity of cobalt molybdate was investigated using electrochemical studies. Electrochemical measurements were performed using cyclic voltammetry and galvanostatic charge discharge measurements. Fig. 4a shows the cyclic voltammetry (CV) curves of cobalt molybdates at the scan rate of 50 mV/s in 3M KOH electrolyte. All cobalt molybdate samples show a pair of redox (anodic and cathodic) peaks. The area under the CV curves was observed to be the highest for CMO-3. Based on the initial observations, detailed electrochemical studies on CMO-3 sample were performed. Fig. 4b shows the CV curves of CMO-3 at various scan rates. It was found that the area under the CV curves increases with increase in scan rates. It is further observed that the peak current increases with increase in the scan rate and the difference in the cathodic and anodic peak potential expands gradually.

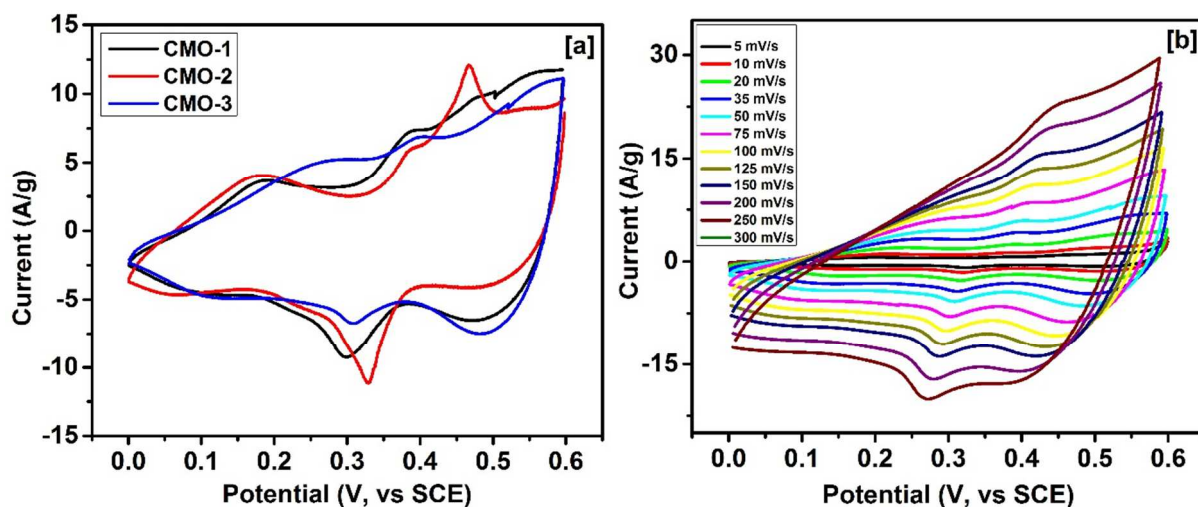


Fig. 4: CV curves of (a) all samples at 50 mV/s in 3M KOH electrolyte, and (b) CMO-3 at various scan rates in 3M KOH electrolyte.

A linear relationship was observed for the peak current and the square root of the scan rate (Fig. 2S). The linear behavior between the peak current and the square root of the scan rate

indicates that the reaction kinetics during the redox process was likely controlled by diffusion processes. The potential application of cobalt molybdate for flexible charge storage device was tested using CV at various bending angles. Fig. 5 shows the CV curves of CMO-3 at various bending angles. The CV curves at various bending angles show identical shape, indicating high electrochemical stability of the cobalt molybdate electrode on bending. The results suggest that cobalt molybdate could have high potential as an electrode material for flexible charge storage devices.

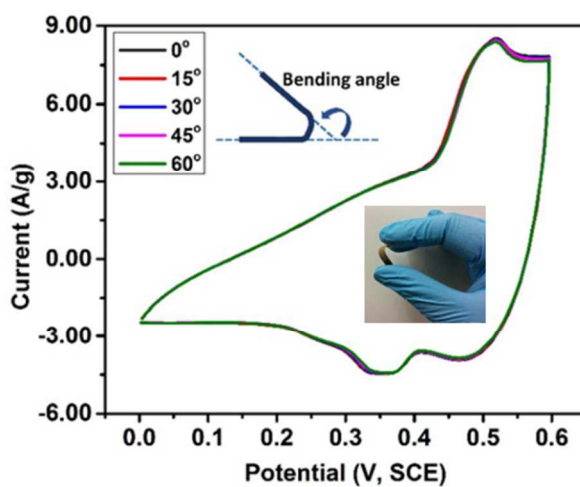


Fig. 5: CV curves of CMO-3 at various bending angles.

The effect of applied current on charge storage capacity of the cobalt molybdates were studied using galvanostatic charge-discharge characteristics. The galvanostatic charge-discharge characteristics of the cobalt molybdates in 3M KOH electrolyte are shown in Fig. 3S. Fig. 6 shows the charge-discharge characteristics of CMO-3 at various applied current in 3M KOH and LiOH electrolytes. As seen in the Fig. 6, the charge-discharge curves are highly symmetric in shapes indicating high electrochemical reversibility and fast reaction kinetics.^{36, 37} In addition to symmetrical charge-discharge profile, it was observed that charge-discharge time depends on the electrolytes. The charge-discharge time (and thus the capacitance) was observed to be maximum

in LiOH electrolyte. This could be due to the smallest ionic size of the Li ions. The smaller ions could approach to the surface of the cobalt molybdate easily and more effectively.

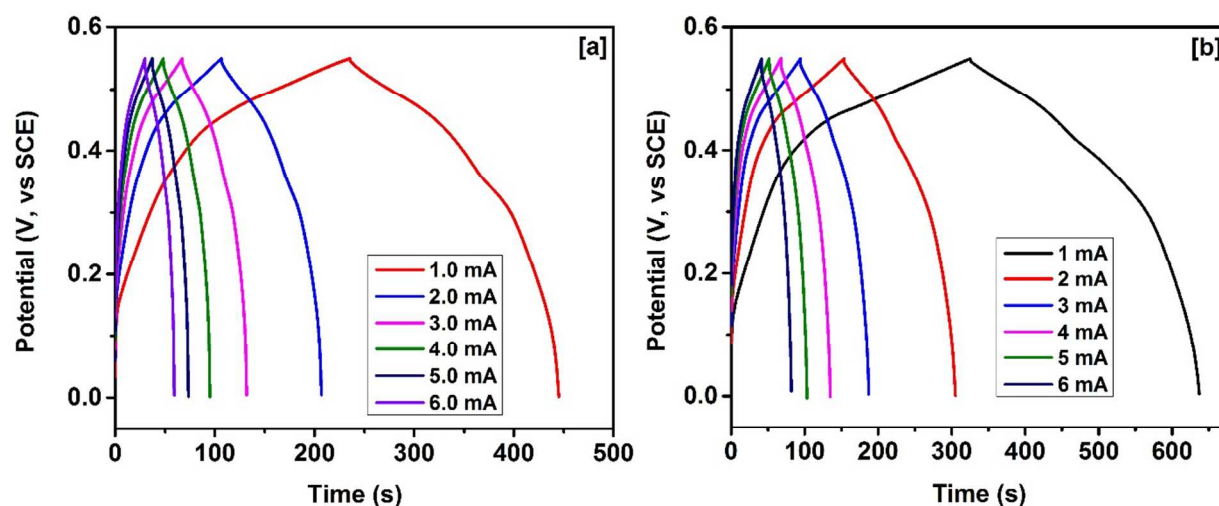


Fig. 6: Galvanostatic charge-discharge characteristics of CMO-3 at different currents in (a) 3M KOH and (b) 3M LiOH electrolyte.

The specific capacitance (C_{sp}) of the cobalt molybdate electrode was calculated using the equation:

$$C_{sp} = \frac{I \times \Delta t}{\Delta V \times m} \quad \dots\dots\dots (3)$$

Where, I is the discharge current (A), Δt is the discharge time (s), ΔV is the potential window (V) and m is the mass (g) of the active material. Fig. 7a shows the variation of specific capacitance versus discharge currents for all the samples in 3M KOH electrolyte. The specific capacitance of the samples decreases with increasing current. The decrease in the specific capacitance with the increase of the discharge current could be due to increase of potential drop and insufficient faradic redox reaction at higher discharge currents. The specific capacitance of 158, 142 and 169 F/g were observed for CMO-1, CMO-2 and CMO-3, respectively at 1 mA of discharge current. Veera subramani et al³³ have used sonochemical method to synthesis

CoMoO₄. They observed a specific capacitance of ~133 F/g in KOH electrolyte. The higher specific capacitance observed for our hydrothermally synthesized CMO-3 could be due to its nanostructure. The nanostructured materials offer higher surface area for redox reactions which results in higher specific capacitance. The effect of ionic size of the electrolytes was also investigated. Fig. 7b shows variation of specific capacitance of CMO-3 with discharge current in different electrolytes. As seen, Li⁺ and Na⁺ have almost similar effect on charge storage capacity. On the other hand KOH electrolyte shows the minimum charge storage compared to LiOH and NaOH which could be due to the largest ionic radius of K⁺.

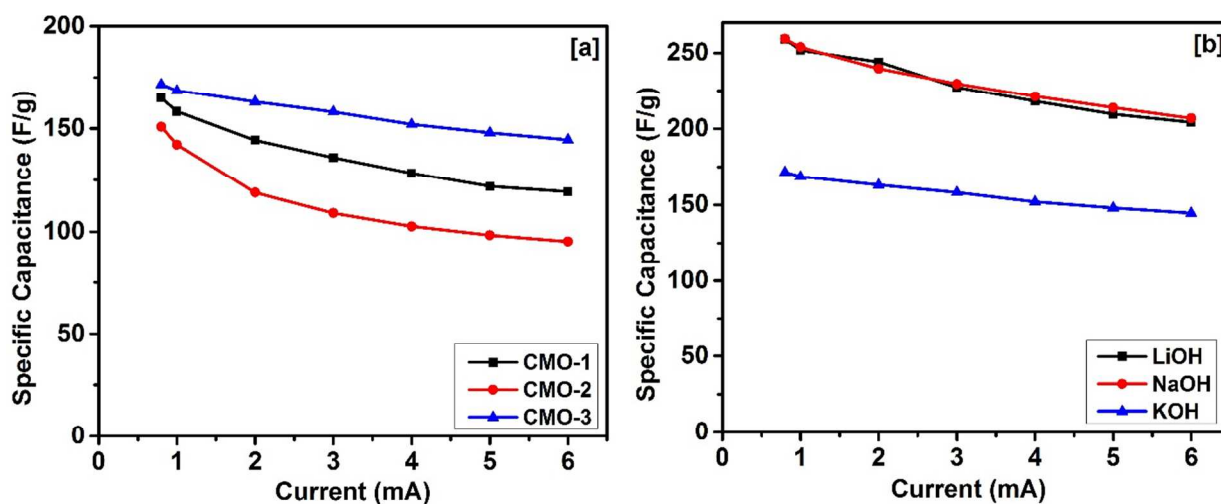


Fig. 7: Variation of specific current versus current for (a) all samples in 3M KOH electrolyte, and (b) CMO-3 in 3M LiOH, NaOH and KOH electrolytes.

The performance of the supercapacitors was further evaluated using a Ragone plot which relates energy density to power density of a material. The energy density and the power density for a supercapacitor cell can be calculated using the following equations:³⁸

$$E \left(\frac{Wh}{kg} \right) = \frac{C_{sp} \times \Delta V^2}{7.2} \dots \dots \dots (4)$$

$$P \left(\frac{W}{kg} \right) = \frac{E \times 3600}{t} \dots\dots\dots (5)$$

Where C_{sp} (F/g) is the specific capacitance calculated from charge-discharge characteristics, ΔV (V) is the potential window and t (s) is the discharge time. In Fig. 8a and 8b, we show the plots of the specific energy density and power density of all the samples measured in 3M KOH electrolyte and CMO-3 in all three electrolytes, respectively. CMO-2 delivers the maximum power density but energy density is low, on the other hand, CMO-3 delivers both very high power density and energy density in LiOH and NaOH electrolytes (Fig. 8b). Veerasubramani et al³³ have reported the values of energy density and power density as 9.06 Wh/kg and 69.9 W/kg at a discharge current density of 1 mA/cm² for sonochemically synthesized cobalt molybdate.

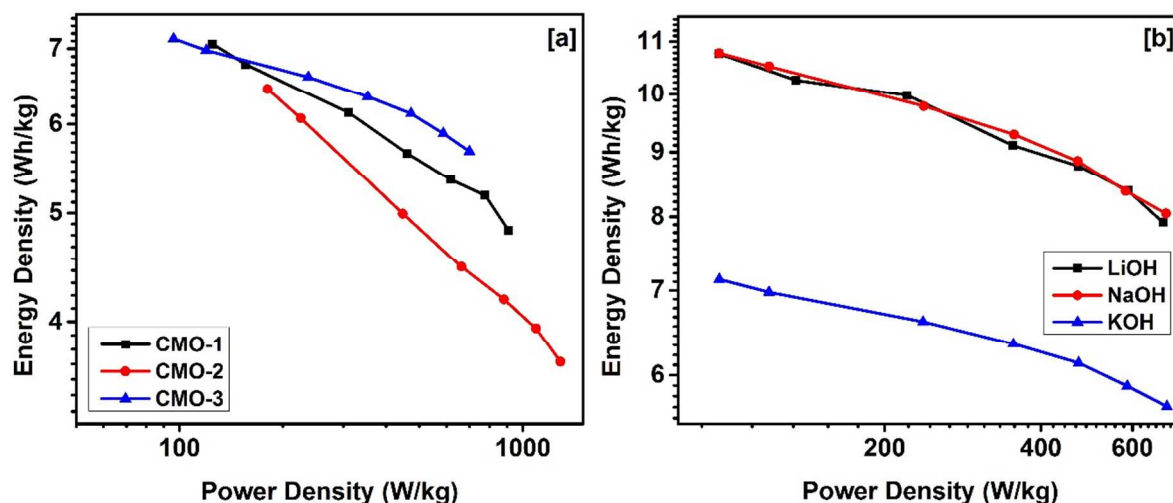


Fig. 8: Variation of power density versus energy density for (a) all samples in 3M KOH electrolyte, and (b) CMO-3 in 3M LiOH, NaOH and KOH electrolytes.

Fig. 9 shows the variation of specific capacitance with charge-discharge cycles for CMO-3 in 3 M NaOH electrolyte. The inset of Fig. 9 shows first few cycles of charge-discharge curves for the same sample. As seen, the specific capacitance of the electrode slowly increases with charge-discharge cycles. The increase in the capacitance with cyclic charge-discharge process

could be due to activation of the cobalt molybdate surface with time. This makes the surface of cobalt molybdate in full contact with the electrolyte which leads to better electrochemical performance.^{35, 39} The results obtained from electrochemical studies legitimate that cobalt molybdate could be used as a high performance material for flexible charge storage devices.

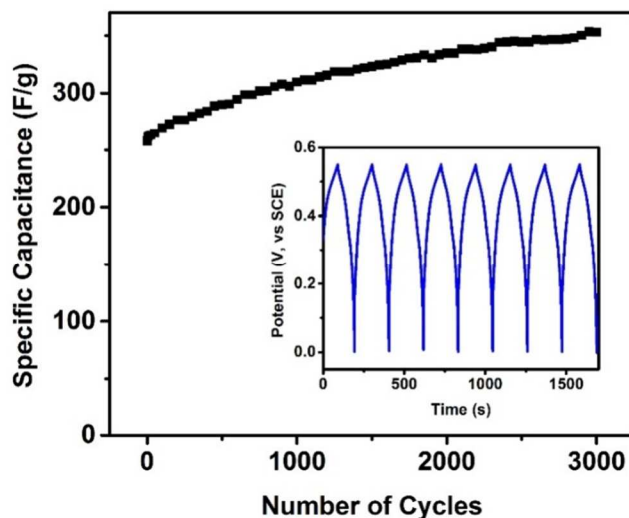


Fig. 9: Variation of specific capacitance versus number of discharge cycles, inset figure shows first few charge-discharge cycles.

The electrochemical properties of the supercapacitor device (Fig. 4S) was studied to investigate its applicability as a flexible device which could operate at elevated temperature. The as fabricated device was lightweight and highly flexible. The CV curves of the device as a function of bending angles are shown in Fig. 10. The device was bended manually at various angles for electrochemical testing. The CV curves demonstrate that there is no significant change (less than 0.5%) in the charge storage capacity of the device on bending which suggest that device can be successfully used as a flexible charge storage device. The effect of scan rate on the CV curves of the device was studied (Fig. 5S). The rectangular shapes and symmetry of the CV

curves indicate near ideal pseudocapacitive nature of the device, even at the high scan rates. The inset of Fig. 5S shows the specific capacitance of the device as a function of scan rates. The specific capacitance (C_{sp}) of the device was calculated using the following expression:⁴⁰

$$C_{sp} = \frac{Q}{\Delta V \times \left(\frac{\partial v}{\partial t}\right) \times A} \dots\dots\dots (6)$$

Where Q is the area under the CV curve, $\partial v/\partial t$ is the scan rate, ΔV is the potential window and A is the area of the device. The specific capacitance of the device decreases from 0.57 to 0.08 F/cm² with increasing scan rate from 10 mV/s to 200 mV/s, respectively. The decrease in the specific capacitance with increase in the scan rate could be due to insufficient time for electrochemical reactions. At higher scan rate the concentration of the ions at the electrode/electrolyte interface is high and diffusion rate of electrolyte from electrode/electrolyte interface to electrode may be not enough to satisfy the electrochemical reactions.⁴¹

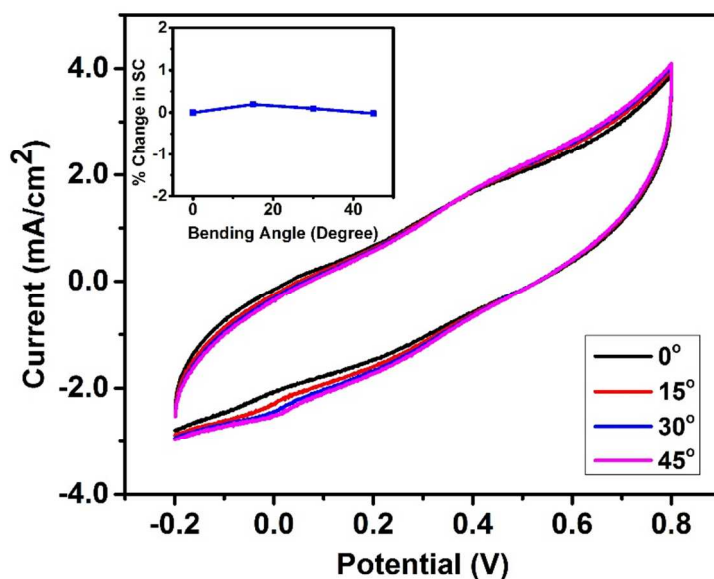


Fig. 10: CV curves of the supercapacitor device at various bending angles. Inset figure shows the change in the specific capacitance (SC) as a function of bending angle.

The long term cyclic stability of the device was studied using cyclic voltammetry. Fig. 11 shows the CV curves of the device at various cycles. The shape and area of the voltammograms were nearly identical, suggesting high cyclic stability of the fabricated device. The inset of Fig. 11 shows percentage retention of specific capacitance as a function of number of cycles. It was observed that the specific capacitance of the device first decreases and then increases up to 3000 cycles. The improved cyclic stability of the device could be due to a gradual access of electrolyte ion to the active sites of the electrode surface with the continuous cycles. Yuan et al⁴² have also observed a similar improvement in the specific capacitance upon cycling for hierarchically porous Co_3O_4 film. Ouassim Ghodbane et al⁴³ have also reported improvement in capacitive properties of electrochemical supercapacitor based on MnO_2 .

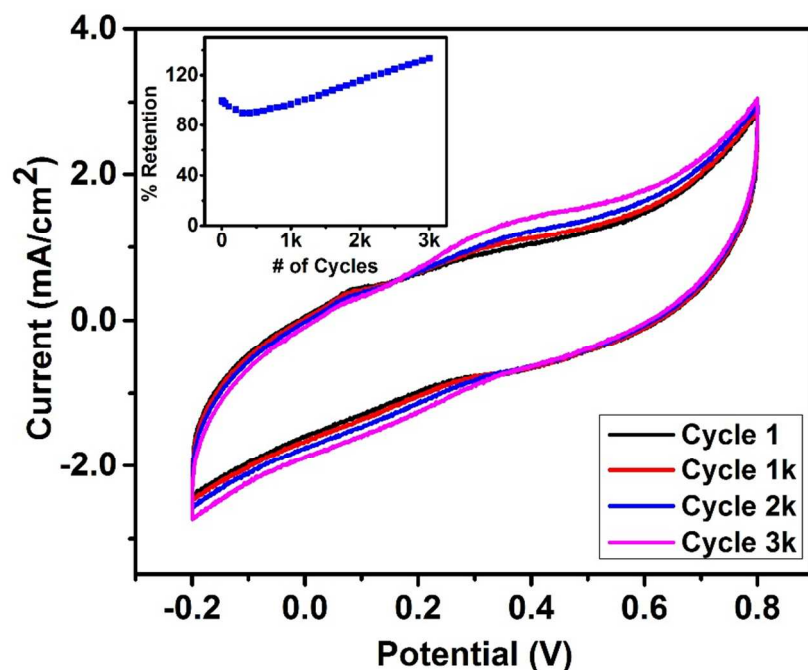


Fig. 11: CV curves of the supercapacitor device at various number of cycles. Inset figure shows % retention of specific capacitance as a function of number of cycles.

Electrochemical properties are dependent on the temperature. Therefore, we have studied the effect of temperature on the charge storage capacity of the device for their applications in harsh temperature environments. Fig. 12 shows the CV curves of the device at various temperatures. The shape of voltammograms are very similar even at higher temperature, indicating near ideal capacitive behavior within this wide temperature window. It was further observed that the specific capacitance of the device increases with increasing temperature. The inset of Fig. 12 shows the percentage increase in the capacitance of the device with temperature. The device showed an increase of 386% in the specific capacitance when the working temperature was increased from 10 to 70 °C. The SEM images of the electrode material before and after electrochemical testing were very similar indicating no structural damage of the cobalt molybdate (Fig. 6S). This indicates that cobalt molybdates are more suitable for charge storage applications at elevated higher temperature rather low temperature conditions.

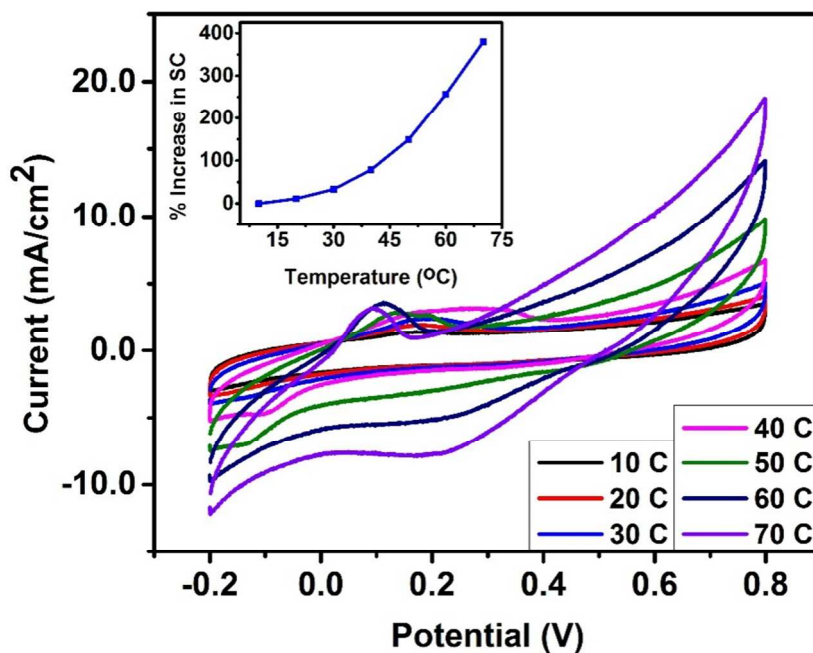


Fig. 12: CV curves of the supercapacitor device at various temperatures. Inset figure shows % increase in specific capacitance of the device with temperature.

The increase in the capacitance of the device with increasing temperature was analyzed using electrochemical impedance spectroscopy (EIS). The main objective of the EIS measurements was to gain insight into the temperature dependence of the resistive and capacitive elements and their effects on the performance of the supercapacitor device. Fig. 13 shows the EIS spectra of the device at various temperatures. As seen in the figure, the equivalent series resistance (ESR) of the device decreases with increasing temperature. The decrease in the ESR value could be due to the enhanced mobility of the ions in the electrolyte which increases the conductivity of the electrolyte.⁴⁴ Therefore, the reduced ESR at higher temperature plays a key role in improving the charge storage capacity of the device. The impedance of the device was also observed to decrease with increasing temperature and frequency (Fig. 7S). Meng et al⁴⁵ have also observed an improvement in the capacitance with temperature for porous Fe₃O₄/carbon composite electrode. The present study indicates that cobalt molybdate could be a promising material for flexible charge storage device with additional advantage of improved charge storage at high temperature.

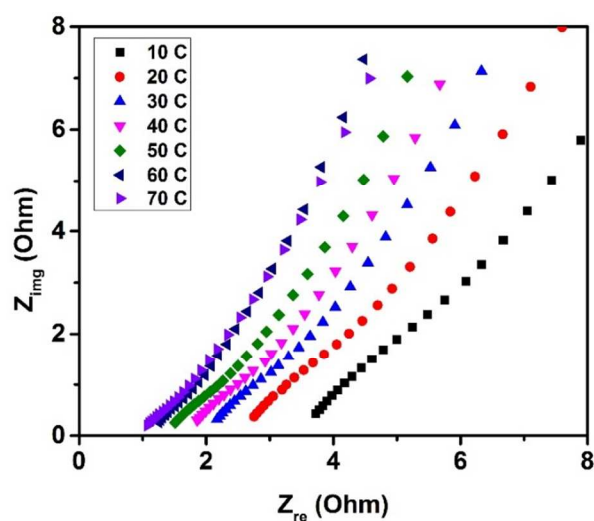


Fig. 13: Z_{re} vs Z_{img} plots (Nyquist plots) of the device at various temperatures.

4. Conclusions

Cobalt molybdates with varying morphology were synthesized using a hydrothermal method. The present study provides a new feature to change in the growth conditions yielded different morphologies such as cauliflower, brick and nano-sphere. The charge storage capacity of these materials were examined using electrochemical techniques. The cyclic voltammograms of the cobalt molybdate electrodes showed a typical pseudocapacitive behavior. The charge storage capacity was observed to depend on the morphology of the cobalt molybdate. The highest specific capacitance of 259 F/g at the current of 1 mA in 3M NaOH was observed with great cyclic stability for the nano-sphered cobalt molybdate. These electrodes showed great flexibility with no degradation in charge-storage capacity. In addition to flexibility, high charge storage capacity and cyclic stability, they offer robust performance at evaluated temperature. The specific capacitance of the cobalt molybdate device showed about 386% improvement in the charge storage capacity when the working temperature was elevated from 10 to 70 °C. Hence, this work provides a new facile method to synthesize morphologies controlled cobalt molybdates for next generation flexible energy storage devices for high-temperature applications.

Acknowledgements

Authors wish to thank Pittsburg State University for providing financial support. This material is based upon work supported by the National Science Foundation under Award No. EPS-0903806 and matching support from the State of Kansas through the Kansas Board of Regents.

References:

1. R. Kötz and M. Carlen, *Electrochim. Acta*, 2000, **45**, 2483-2498.
2. Y. Zhang, H. Feng, X. Wu, L. Wang, A. Zhang, T. Xia, H. Dong, X. Li and L. Zhang, *Int. J. Hydrogen Energy*, 2009, **34**, 4889-4899.
3. A. Burke, *Electrochim. Acta*, 2007, **53**, 1083-1091.
4. H. R. Ghenaatian, M. F. Mousavi and M. S. Rahmanifar, *Synth. Met.*, 2011, **161**, 2017-2023.
5. B. E. Conway, V. Birss and J. Wojtowicz, *J. Power Sources*, 1997, **66**, 1-14.
6. J.-L. Shi, W.-C. Du, Y.-X. Yin, Y.-G. Guo and L.-J. Wan, *Journal of Materials Chemistry A*, 2014, **2**, 10830-10834.
7. A. Burke, *J. Power Sources*, 2000, **91**, 37-50.
8. C. Ashtiani, R. Wright and G. Hunt, *J. Power Sources*, 2006, **154**, 561-566.
9. A. Chu and P. Braatz, *J. Power Sources*, 2002, **112**, 236-246.
10. A. Burke and M. Miller, *J. Power Sources*, 2011, **196**, 514-522.
11. T. Chen and L. Dai, *Journal of Materials Chemistry A*, 2014, **2**, 10756-10775.
12. E. Mitchell, R. K. Gupta, K. Mensah-Darkwa, D. Kumar, K. Ramasamy, B. K. Gupta and P. Kahol, *New J. Chem.*, 2014, **38**, 4344-4350.
13. E. Mitchell, F. De Souza, R. K. Gupta, P. K. Kahol, D. Kumar, L. Dong and B. K. Gupta, *Powder Technol.*, 2015, **272**, 295-299.
14. H. Wang, Y. Wang and X. Wang, *New J. Chem.*, 2013, **37**, 869-872.
15. J. Chen, K. Huang and S. Liu, *Electrochim. Acta*, 2009, **55**, 1-5.
16. L. Yang, S. Wang, J. Mao, J. Deng, Q. Gao, Y. Tang and O. G. Schmidt, *Advanced Materials*, 2013, **25**, 1180-1184.
17. Y. Gao, S. Chen, D. Cao, G. Wang and J. Yin, *J. Power Sources*, 2010, **195**, 1757-1760.
18. L. Qian, L. Gu, L. Yang, H. Yuan and D. Xiao, *Nanoscale*, 2013, **5**, 7388-7396.
19. U. M. Patil, S. B. Kulkarni, V. S. Jamadade and C. D. Lokhande, *J. Alloys Compd.*, 2011, **509**, 1677-1682.
20. P. M. Kulal, D. P. Dubal, C. D. Lokhande and V. J. Fulari, *J. Alloys Compd.*, 2011, **509**, 2567-2571.
21. J.-G. Wang, Y. Yang, Z.-H. Huang and F. Kang, *J. Power Sources*, 2012, **204**, 236-243.
22. W.-H. Jin, G.-T. Cao and J.-Y. Sun, *J. Power Sources*, 2008, **175**, 686-691.
23. X. Yan, X. Tong, J. Wang, C. Gong, M. Zhang and L. Liang, *J. Alloys Compd.*, 2014, **593**, 184-189.
24. Y. Hou, L. Chen, P. Liu, J. Kang, T. Fujita and M. Chen, *Journal of Materials Chemistry A*, 2014, **2**, 10910-10916.
25. Y. Qian, R. Liu, Q. Wang, J. Xu, D. Chen and G. Shen, *Journal of Materials Chemistry A*, 2014, **2**, 10917-10922.
26. Y. Liu, J. Zhang, S. Wang, K. Wang, Z. Chen and Q. Xu, *New J. Chem.*, 2014, **38**, 4045-4048.
27. J. Feng, X. Sun, C. Wu, L. Peng, C. Lin, S. Hu, J. Yang and Y. Xie, *J Am Chem Soc*, 2011, **133**, 17832-17838.
28. K. Krishnamoorthy, G. K. Veerasubramani, S. Radhakrishnan and S. J. Kim, *Chem Eng J*, 2014, **251**, 116-122.
29. D. Cai, B. Liu, D. Wang, Y. Liu, L. Wang, H. Li, Y. Wang, C. Wang, Q. Li and T. Wang, *Electrochim. Acta*, 2014, **115**, 358-363.

30. L.-Q. Mai, F. Yang, Y.-L. Zhao, X. Xu, L. Xu and Y.-Z. Luo, *Nat Commun*, 2011, **2**, 381.
31. D. Cai, D. Wang, B. Liu, Y. Wang, Y. Liu, L. Wang, H. Li, H. Huang, Q. Li and T. Wang, *ACS Applied Materials & Interfaces*, 2013, **5**, 12905-12910.
32. X. Xia, W. Lei, Q. Hao, W. Wang and X. Wang, *Electrochim. Acta*, 2013, **99**, 253-261.
33. G. K. Veerasubramani, K. Krishnamoorthy, S. Radhakrishnan, N.-J. Kim and S. J. Kim, *Int. J. Hydrogen Energy*, 2014, **39**, 5186-5193.
34. X. Xu, J. Shen, N. Li and M. Ye, *J. Alloys Compd.*, 2014, **616**, 58-65.
35. M.-C. Liu, L.-B. Kong, X.-J. Ma, C. Lu, X.-M. Li, Y.-C. Luo and L. Kang, *New J. Chem.*, 2012, **36**, 1713-1716.
36. F. Zhao, Y. Wang, X. Xu, Y. Liu, R. Song, G. Lu and Y. Li, *ACS Applied Materials & Interfaces*, 2014, **6**, 11007-11012.
37. L.-J. Xie, J.-F. Wu, C.-M. Chen, C.-M. Zhang, L. Wan, J.-L. Wang, Q.-Q. Kong, C.-X. Lv, K.-X. Li and G.-H. Sun, *J. Power Sources*, 2013, **242**, 148-156.
38. C. Xiang, M. Li, M. Zhi, A. Manivannan and N. Wu, *J. Power Sources*, 2013, **226**, 65-70.
39. W. Tang, S. Tian, L. L. Liu, L. Li, H. P. Zhang, Y. B. Yue, Y. Bai, Y. P. Wu and K. Zhu, *Electrochem. Commun.*, 2011, **13**, 205-208.
40. J. Gomez and E. E. Kalu, *J. Power Sources*, 2013, **230**, 218-224.
41. S. H. Mujawar, S. B. Ambade, T. Battumur, R. B. Ambade and S.-H. Lee, *Electrochim. Acta*, 2011, **56**, 4462-4466.
42. Y. F. Yuan, X. H. Xia, J. B. Wu, X. H. Huang, Y. B. Pei, J. L. Yang and S. Y. Guo, *Electrochem. Commun.*, 2011, **13**, 1123-1126.
43. O. Ghodbane, J.-L. Pascal and F. Favier, *ACS Applied Materials & Interfaces*, 2009, **1**, 1130-1139.
44. W. Li, K. Xu, L. An, F. Jiang, X. Zhou, J. Yang, Z. Chen, R. Zou and J. Hu, *Journal of Materials Chemistry A*, 2014, **2**, 1443-1447.
45. W. Meng, W. Chen, L. Zhao, Y. Huang, M. Zhu, Y. Huang, Y. Fu, F. Geng, J. Yu, X. Chen and C. Zhi, *Nano Energy*, 2014, **8**, 133-140.